Comparative microfluidic screening of amino acid salt solutions for post-combustion CO_2 capture

Alexander P. Hallenbeck[a,b], Adefemi Egbebi[a,c], Kevin P. Resnik[a,c], David Hopkinson[a], Shelley L. Anna[b], John R. Kitchin[a,b,*]

[a] *National Energy Technology Laboratory, Pittsburgh Pennsylvania, 15236*
[b] *Department of Chemical Engineering, Carnegie Mellon University, Pittsburgh, PA 15213*
[c] *AECOM, Pittsburgh, PA, 15236*

Abstract

The CO_2 absorption capacity and rate of aqueous solutions of MEA and the potassium salts of glycine, taurine, proline, and lysine were compared in a microfluidic device. These properties were measured by tracking the volume change of an entrained CO_2 gas plug as it traveled through a microfluidic channel. The potassium salt of lysine, which contains two primary amine functional groups, exhibited the highest rich CO_2 loading, >50% higher than MEA. The salts of glycine, and taurine exhibited similar absorption capacity to MEA, and the salt of proline exhibited the lowest absorption capacity. The trend in absorption capacities of the potassium salt of lysine and MEA was also observed in a set of breakthrough CSTR experiments. Raman spectroscopy was used to analyze the absorbent solutions before exposure to CO_2 as well as the reactor effluent. Spectral features of carbamate, carbonate, and bicarbonate were identified in the effluent spectra. The effectiveness of the microfluidic reactor as a solvent volume and time efficient screening tool is

*Corresponding author
Email address: jkitchin@andrew.cmu.edu (John R. Kitchin)

demonstrated. The results suggest further work should be done to evaluate the efficacy of the alkali salt of lysine as a post-combustion CO_2 capture absorbent as it has potential to match or possibly improve upon the CO_2 loading of MEA while offering advantages such as low toxicity and lower volatility.

Keywords: Lysine, Segmented flow, Raman, Microfluidic

1. Introduction

The combustion of fossil fuels such as coal, oil, and natural gas for energy is responsible for a significant fraction of CO_2 emissions [1]. Specifically, 38% of the total U.S. CO_2 emissions in 2012 were due to electricity generation [2]. Post-combustion carbon capture and sequestration is a potential approach to mitigating the impact of these CO_2 emissions that would allow the current infrastructure to remain largely intact while continued research into alternative fuels and energy production is done [3].

The most mature technology for post-combustion CO_2 capture is absorption via an aqueous solution of 30 wt% monoethanolamine (MEA) solution using an absorber and stripper to capture CO_2 cyclically [4]. Amine solvents, including MEA, react reversibly and exothermically with CO_2 to form an amine-CO_2 complex. This complex is typically either a carbamate or a bicarbonate depending on the structure of the amine, with primary and secondary amines preferring the formation of carbamate [5]. While MEA is the industry standard due to its fast reaction kinetics and high CO_2 capacity, there are several drawbacks to its use, including a high regeneration energy cost, solvent loss to oxidative degradation [6] and volatility [7], as well

as its high toxicity and corrosivity. Consequently, a major focus of current research is alternative aqueous-based solvents containing piperazine [8], promoted carbonate solutions [9, 10, 11], and aqueous amino acid salt solutions [12, 13, 14, 15] among others. An alternative approach that has been investigated for a non-aqueous solvent include amine-functionalized ionic liquids [16].

Great interest has been generated in aqueous solutions of amino acid salts as a class of post-combustion CO_2 capture solvents because they have many favorable characteristics. Dissolved amino acids at neutral pH exist in the form of a zwitterion as seen in equation (1).

$$H_3{}^+N{-}CHR{-}COO^- \tag{1}$$

Consequently, the amine group of the amino acid is protonated and unavailable to react with CO_2. However, deprotonating the amine group with a metal hydroxide to form a salt (equation (2)) allows CO_2 to react with the amino acid along amine-CO_2 reaction pathways.

$$H_2N{-}CHR{-}COO^-M^+ \tag{2}$$

We refer to the salt of lysine as lysinate (LYS), the salt of glycine as glycinate (GLY), the salt of taurine as taurinate (TAU), and the salt of proline as prolinate (PRO). Potassium is the most commonly reported cation for CO_2 capture studies [17].

Aqueous amino acid salt solutions have very low volatility (of the amino acids) and high surface tension due to their ionic nature. They react with CO_2 through the same amine functional groups present in alkanolamines.

They have been shown to exhibit excellent oxidative and thermal stability as well as similar capture capacity and kinetics to alkanolamines [18, 19, 20]. Additionally, they are naturally abundant and the R-group presents tunability to the solvent selection. Consequently many investigations have been carried out to assess the efficacy of amino acid salt solutions for CO_2 capture.

Holst et. al. investigated the kinetics of several aqueous solutions of amino acid salts including those of 6-aminohexanoic acid, beta-alanine, l-arginine, l-glutamic acid, dl-methionine, l-proline, and sarcosine [13]. Kinetic experiments were carried out in a closed stirred-cell reactor at a temperature of 298 K and an amino acid salt concentration of 0.5 M. The potassium salts of l-proline and sarcosine were found to be most promising due to their fast kinetics and low pKa.

Kumar et. al. measured the kinetics of the reaction of CO_2 with aqueous potassium salts of taurine and of glycine using a stirred cell reactor with a flat gas-liquid interface [21]. They found that the experimental data could be explained with the same zwitterion mechanism used to interpret the kinetics of CO_2 absorption with primary alkanolamines despite a few differences in kinetic behavior. Unlike for alkanolamines, the partial reaction order in amino acid salt changes from one at low salt concentration to approximately 1.5 at high salt concentration (as high as 3 M). Additionally the forward second order rate constant of the zwitterion mechanism was found to be significantly higher for the amino acid salts than for alkanolamines with similar basicity. Lastly, it was also found that water makes a larger contribution to the deprotonation of the zwitterion in the case of amino acids in comparison

to alkanolamines.

More recently, the kinetics of CO_2 absorption in an aqueous solution of potassium prolinate were measured with a wetted wall reactor [14]. In this work, the authors reported higher second order rate constants for this solvent than for some alkanolamines, and for some other amino acid salts.

Aqueous amino acid salt solutions have also been investigated both experimentally and computationally at the process scale. Siemens has developed a post-combustion CO_2 capture process based on the use of an amino acid salt solution [12]. Process models were used to optimize the CO_2 capture process and predicted an efficiency loss of only 9% in comparison to a standard coal-fired plant [12]. A pilot plant was commissioned to start process validation and solvent optimization in August, 2009 [12]. Knuutila et. al. also investigated the potassium salt of sarcosine with a series of pilot plant experiments and simulations for a salt concentration of 3.5 M. Their results indicated a high absorption rate and high energy requirement for the amino acid salt solution in comparison with 30 wt% MEA [22].

One group of amino acids which has received limited attention are the amino acids with basic side-chains, such as histidine, arginine, and lysine. These amino acids contain additional nitrogen group(s) which depending on the solution conditions (pH) can participate in the reactions with CO_2 increasing the rich CO_2 loading of the solvent. Past work has shown for the case of arginine that the rich CO_2 loading is on order 1 mole CO_2 per mole of arginine, but at the expense of a higher lean CO_2 loading and consequently a working capacity not significantly different from single amine containing molecules such as MEA [23]. Lysine is another amino acid which has only

been included in one previous study that showed it to be very promising to replace and improve upon MEA [24]. Consequently the present work aims to further compare the CO_2 absorption of LYS with MEA and three other amino acid salts that have received extensive attention: GLY, PRO, and the synthetic amino acid salt: TAU. The structures of each amino acid can be seen in Figure 1.

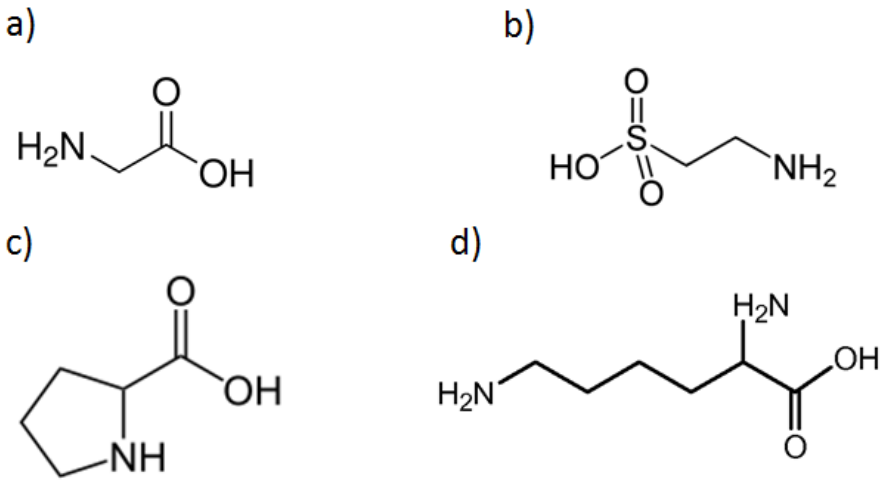

Figure 1: Molecular structure of a) Glycine, b) Taurine, c) Proline, d) Lysine.

Multi-phase microfluidic reactors have recently garnered much attention for the study of rapid chemical reactions. Microfluidic devices have been used in several recent studies on CO_2 physical solubility and mass transfer rate in pre-combustion capture solvents [25, 26, 27, 28] as well as CO_2 absorption by amines [29, 30, 31, 32, 33]. Absorption at microfluidic length-scales occurs through a well-defined two-phase interface and with a high surface area to volume ratio. In addition to the low, 1 mL or less, volume requirements,

microfluidic experiments also significantly reduce the time and complexity of CO_2 absorption experiments over conventional methods such as wetted-wall column and stirred cell reactor experiments. Consequently microfluidics is a very appropriate tool for screening new CO_2 absorbent solutions. The present work will determine the CO_2 uptake of the aqueous amino acid salt solutions through the time dependent decrease in the volume of entrained CO_2 plugs in a microfluidic channel.

2. Materials and Methods

Amino acids were purchased from Sigma Aldrich at purities of at least 98.5%, potassium hydroxide was purchased with a purity of 99.9%,and MEA was purchased with a purity of 99%. All reagents were used without further purification. Deionized water was used for all solutions. Amino acid salt solutions were prepared by neutralizing the amino acid with an equimolar amount of potassium hydroxide. The actual concentration of the aqueous amino acid salt was verified through titration with a 12.1 N HCl solution (Fischer Scientific) using an Orion 4star pH meter. The concentrations of all solutions were 0.50 M with the exception of potassium lysinate which was 0.53 M. CO_2 gas was supplied from a cylinder (Matheson gas) at a 99.995% purity.

2.1. Microfluidic apparatus

Microfluidic experiments were carried out with a commercially available all-glass microreactor from Micronit (product code: FC-R150.676.2_PACK). The reactor contains two inlets, a Y-junction, and a serpentine channel. All inlet and outlet connections were made with the Fluidic Connect Pro chip

holder purchased from Micronit (product code: FC_PRO_CH4515). The flow rate of liquid into one inlet was controlled with a Harvard apparatus phd2000 syringe pump and gas was supplied to the other inlet with a ControlAir type 550x electronic to pneumatic transducer with a supply pressure range of 35 to 100 psig and an outlet pressure range of 0 to 30 psig. Experiments were conducted on a light table with a Nikon Motion pro-x high speed camera. The gas pressure was kept constant at 1.7 atm for all experiments and the liquid flow rate was adjusted in each experiment to obtain a steady production of entrained gaseous plugs at the Y-junction of the microfluidic device as can be seen in Figure 2.

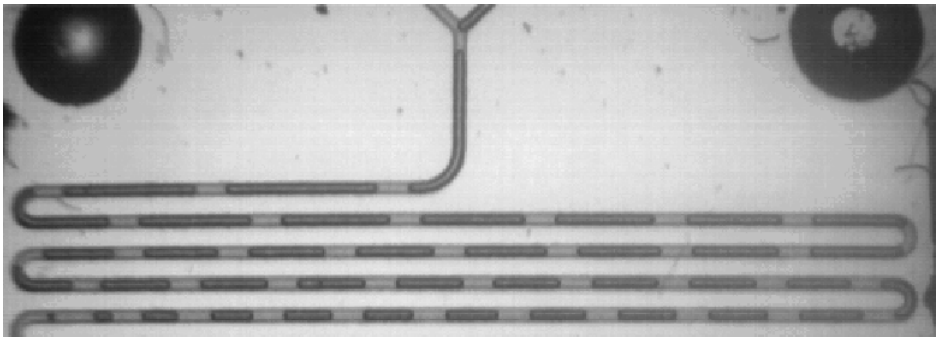

Figure 2: Example image used for analysis of 0.50 M K^+GLY^-.

In each experiment a video was acquired with a frame rate of 500 Hz. This frame rate is sufficiently high to allow for the tracking of the size of an individual gas plug through time as it travels through the reactor. In order to measure the amount of absorbed CO_2, the length of an individual gas plug was measured as the gas plug traveled along the reactor channel using the ImageJ software and can be seen in Figure 3. The gas plug was selected to maintain a constant adjacent liquid slug length (approximately 350 μm)

between all experiments.

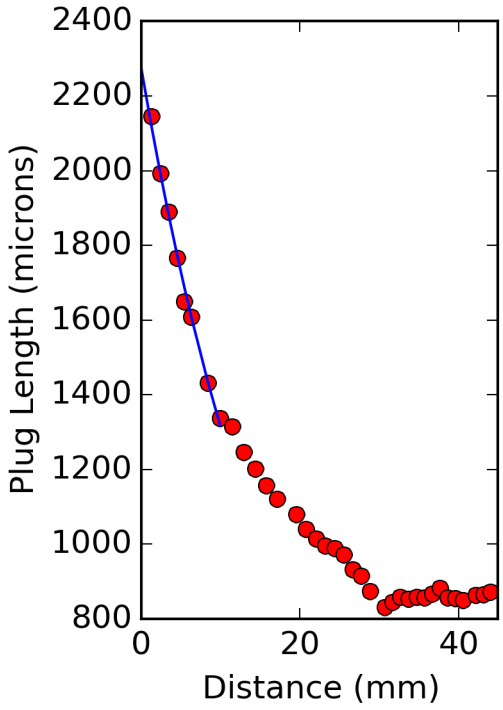

Figure 3: Plug length vs distance used for analysis of 0.50 M K^+GLY^- with exponential fit for determining initial plug length. The initial gas plug length was determined to be 2276 μm.

The initial gas plug length was determined by extrapolating the gas plug length to the y-junction through an exponential fit as can be seen in Figure 3. The volume of a gas plug was calculated assuming a plug consisting of a cylinder and two hemispherical endcaps. Previous work [29] with the same microreactor determined the hydraulic diameter of the microchannel to be 125 μm through confocal fluorescence microscopy. We assumed the hydraulic diameter of each gas plug to be 121 μm to account for the thin liquid film

between the plug and reactor walls as was done in Li et. al. The moles of absorbed CO_2 was then determined by applying the ideal gas law based on the measured ambient temperature (294-296K). The precision of the resulting concentration data is within 0.02 M based on propogating the precision of the plug and slug length measurements.

2.2. Raman Spectroscopy

Raman spectroscopy was carried out with the prepared absorbent solutions prior to microfluidic experiments and with a sample of the microreactor effluent following each microfluidic experiment. Raman spectra were acquired with a Horiba LabRamHR spectrometer using a Spectra Physics 532 nm Nd:Yag laser with an operating power of 0.2 W as the excitation source. Spectra were taken using an Olympus 50xLWD objective and were recorded as an average of 10 three second exposures over each spectral range. Prior to each set of measurements, the spectrometer was calibrated using a silicon standard.

2.3. CSTR

The CO_2 absorption testing unit is a continuously stirred reactor vessel (300 ml EZE-Seal Stirred Reactor from Autoclave Engineers). It is equipped with a set of mass flow controllers (MFCs) allowing for control of up to five different gases/mixtures, which can be blended and directed into a single gas inlet port at the top of the reactor. Gases are introduced into the reactor via a diptube connected to the gas inlet port. Solvent is pre-loaded into the vessel, where it is continuously stirred with the impeller for adequate mixing and mass transfer. Gaseous products exit the reactor at the top through a

single gas outlet port and immediately directed into a cold trap to condense out the vapor leaving the reactor with the gases. After the cold trap, the gas stream passes through a back pressure regulator (BPR) prior to being vented. A slipstream of the gas stream is constantly being withdrawn via a capillary connection for gas analysis by a Dycor® series Dymaxion Residual Gas Analyzer (RGA) from AMETEK.

For equilibrium CO_2 absorption measurements, the solvent is loaded into the vessel and sealed. N_2 gas is briefly directed into the vessel to purge air/O_2 from the system. The vessel is then isolated while the solvent is constantly stirred as it is gradually brought up to the 40 °C absorption temperature with the heater. At the same time the gas feed, now bypassing the vessel, is changed to 14% CO_2/N_2 at the desired flow rate to establish steady flow as measured by the RGA. When both the absorption temperature and flow rate is attained, the vessel is brought back online to start the absorption test. The solvent is saturated and equilibrium reached when the concentration of gas exiting the vessel is equal to the initial concentration as recorded by the RGA. RGA data is reduced and numerically integrated to calculate the amount of CO_2 absorbed by the solvent.

3. Results

3.1. Microfluidic experiments

Microfluidic absorption experiments were carried out at ambient temperature with a gas delivery pressure of 1.7 atm for MEA and GLY, TAU, PRO at a concentration of 0.50 M and for LYS at a concentration of 0.53 M. The size of a specific CO_2 gas plug was monitored as a function of time starting at

the Y-junction and the molar concentration of absorbed CO_2 in the adjacent liquid slugs was calculated as described above. The resulting concentration of absorbed CO_2 can be seen in Figure 4 for all of the studied solutions.

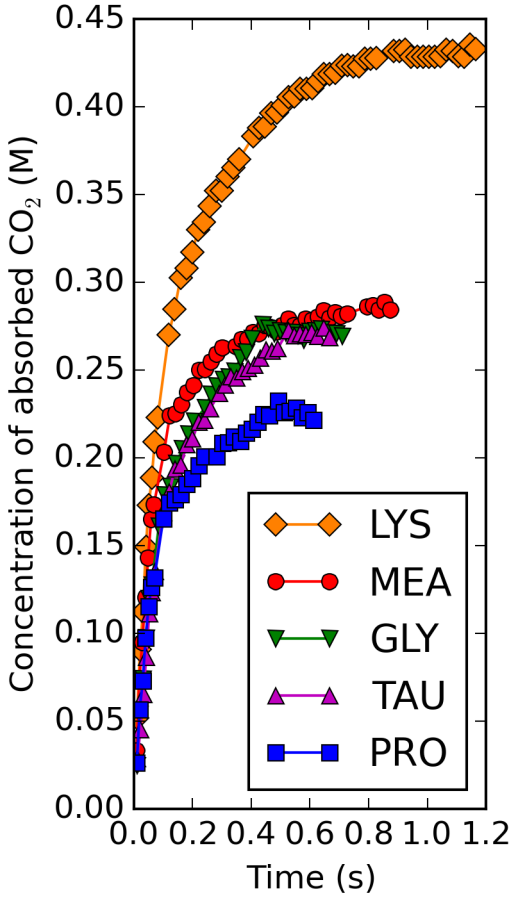

Figure 4: Concentration of absorbed CO_2 during microfluidic experiments as a function of time.

Since the partial pressure of CO_2 is significantly lower in the typical post-combustion flue gas, the physical solubility of CO_2 in the amine solution is

typically negligible. Consequently, the reacted CO_2 loading was calculated by approximating the physical solubility of CO_2 in the amine or amino acid salt solution with that of water. The CO_2 loadings after subtracting the physical solubility can be seen below in Table 1.

Table 1: Maximum reacted CO_2 loadings during MF experiments.

Solvent	CO_2 loading (mol CO_2/mol Am)
LYS	0.70
MEA	0.46
GLY	0.43
TAU	0.43
PRO	0.34

As an arbitrary metric for comparing the absorption rates, the time to reach 90% of the above maximum CO_2 loadings was measured and can be seen in Table 2.

Table 2: Time to reach 90% of maximum CO_2 loading during MF experiments.

Solvent	t (s)
MEA	0.30
GLY	0.34
PRO	0.34
TAU	0.37
LYS	0.47

Another metric for comparing the absorption rates is to compare the initial absorption flux as calculated over the initial 0.02 s of the absorption

assuming the mass transfer area is approximately the area of the endcaps of the gas plug.

Solvent	Initial absorption flux ($mol*m^{-2}*s^{-1}$)
LYS	0.52
MEA	0.48
PRO	0.35
GLY	0.32
TAU	0.25

3.2. CSTR

In order to determine the effectiveness of the microfluidic experiments in predicting the trends in CO_2 loading and rate at larger macroscale and industrially relevant volumes and solvent concentrations a set of equilibrium CO_2 absorption experiments were conducted with a 300 mL CSTR. The equilibrium CO_2 absorption capacities of potassium lysinate and MEA were determined from integration of the CO_2 breakthrough curves. Samples of the same composition as in the microfluidic experiments were measured as well as a 30 wt% MEA solution and 1.48M(or equivalently 70 wt% H_2O) potassium lysinate in order to compare the two solutions with a constant weight fraction of water. Experiments were conducted at 313.15 K and from a 10 vol% CO_2 gas stream for the low solvent concentration experiments and 14 vol% CO_2, balance N_2, gas stream for the high solvent concentration experiments. The cumulative amount of absorbed CO_2 throughout each experiment can be seen in Figure 5 (0.5M), and Figure 6 (70wt% water).

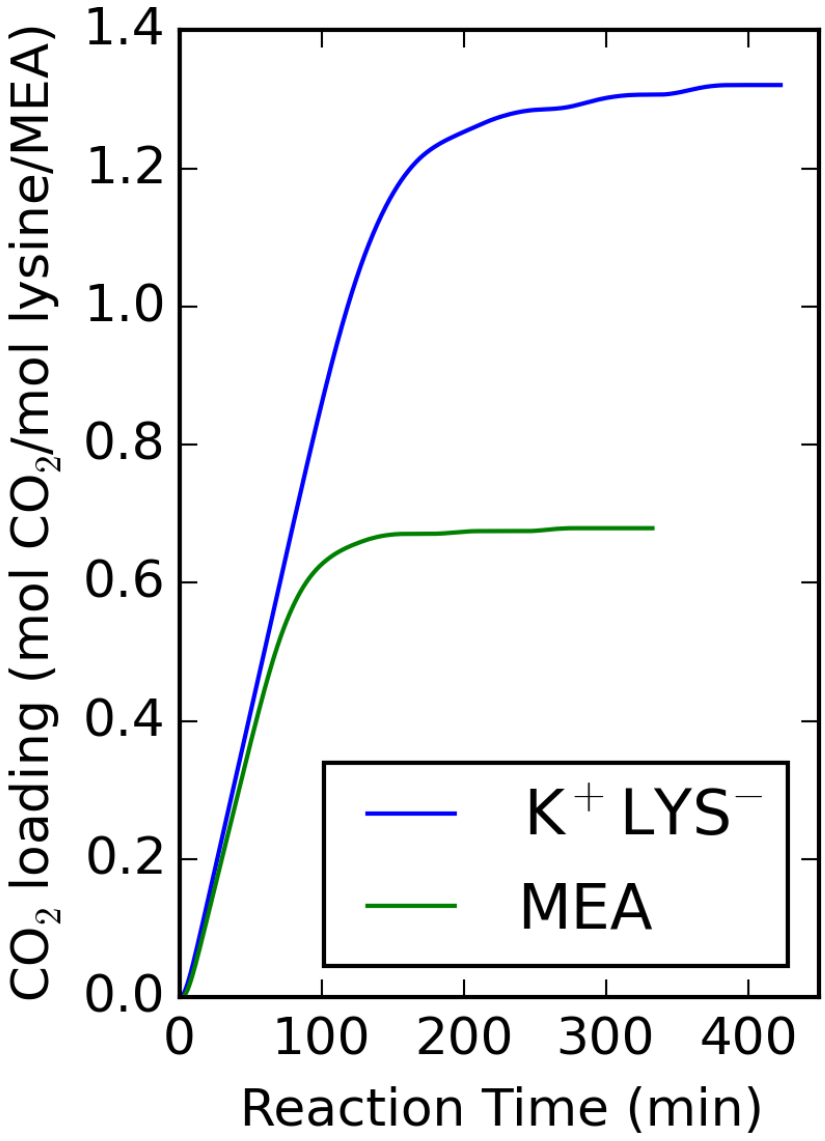

Figure 5: Cumulative CO_2 loading throughout CSTR breakthrough for 0.5M K^+LYS^- and MEA.

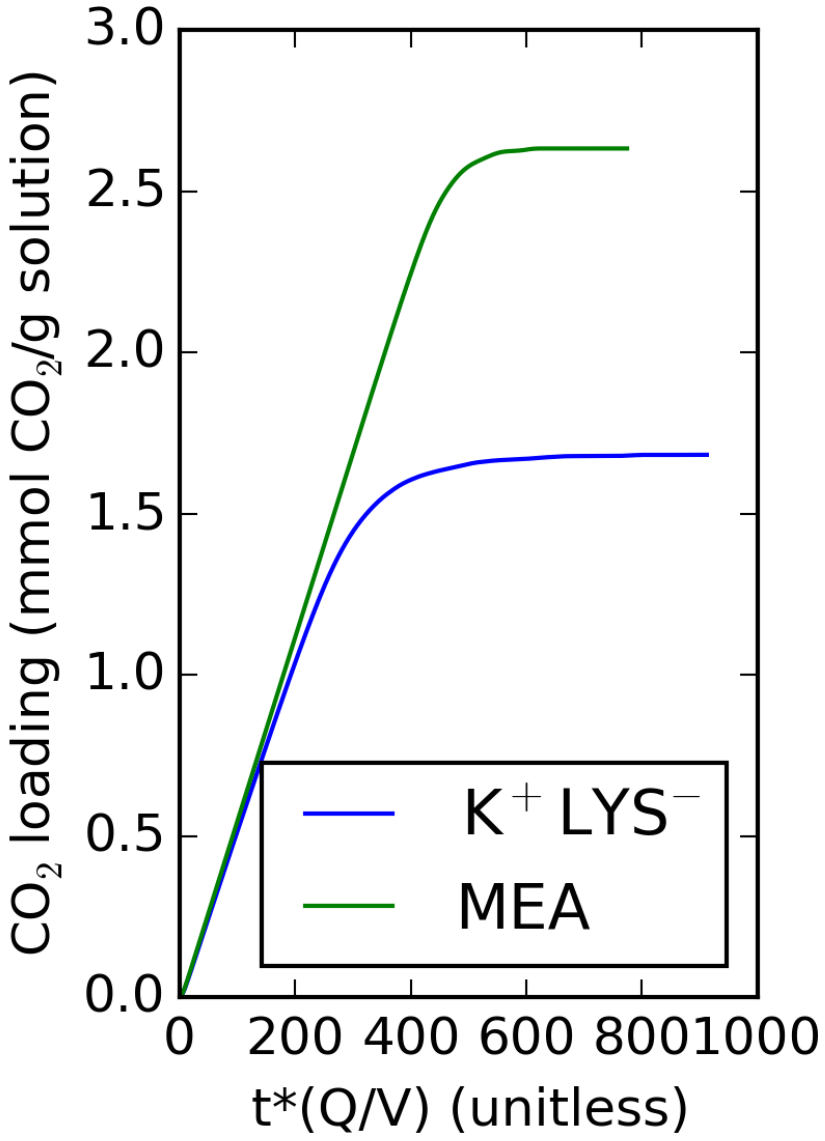

Figure 6: Cumulative CO_2 loading throughout CSTR breakthrough for 1.48M K^+LYS^- and 30 wt% MEA.

A comparison of the equilibrium absorption capacities can be seen in

Table 3

Table 3: Equilibrium CO_2 loadings during CSTR experiments.

Solvent	CO_2 loading (mol CO_2/mol MEA/Lysine)	CO_2 loading (mmol/g solution)
0.53M LYS	1.32	0.68
0.53M MEA	0.70	0.37
1.48M LYS	1.19	1.68
30wt% MEA	0.53	2.63

The viscosities of the 1.48M LYS solution and the 30 wt% MEA solution was determined by a RheoSense micro viscometer. The viscosities were nearly identical as can be seen in Tables 4 — 5

Table 4: Viscosity of 1.48M Potassium Lysinate.

Temperature (K)	Viscosity (mPas)
293.14	3.078
293.13	3.069
303.29	2.27
313.21	1.723

Table 5: Viscosity of 30 wt% MEA.

Temperature (K)	Viscosity (mPas)
293.17	3.159
293.16	3.161
303.22	2.277
313.03	1.751

These values are consistent with previously reported viscosity measurements of 30 wt% MEA solution [**?**].

3.3. Raman Spectroscopy

Raman spectra for each absorbent solution both before and after absorbing CO_2 in the microfluidic reactor can be seen below in Figures 7 — 11.

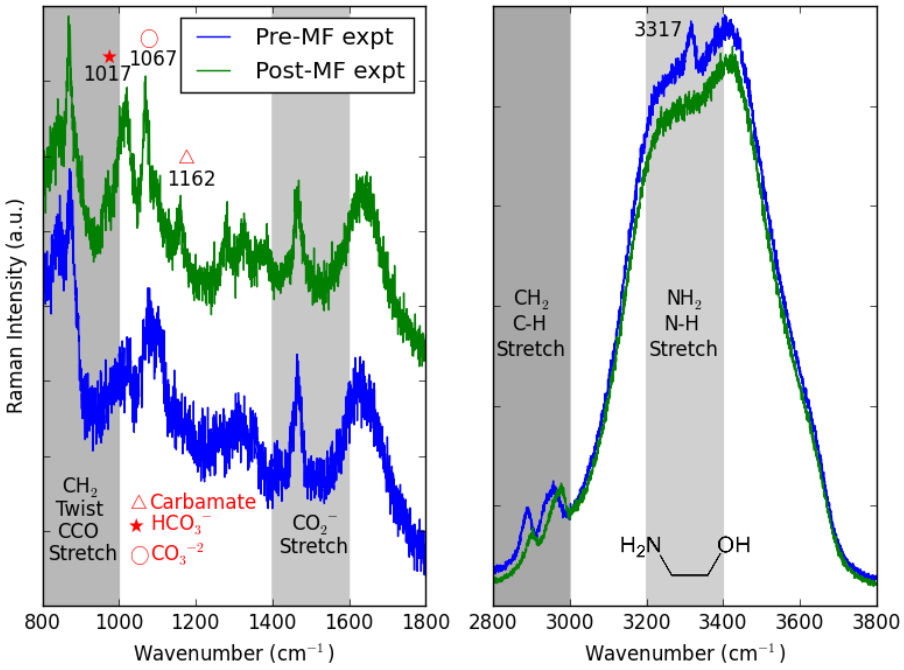

Figure 7: Raman Spectra for MEA.

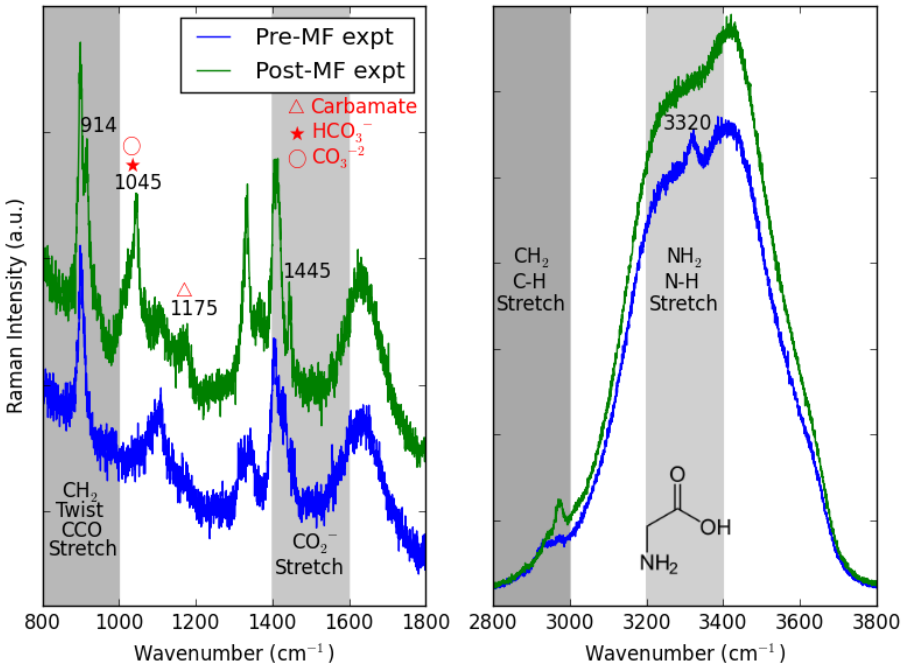

Figure 8: Raman Spectra for GLY.

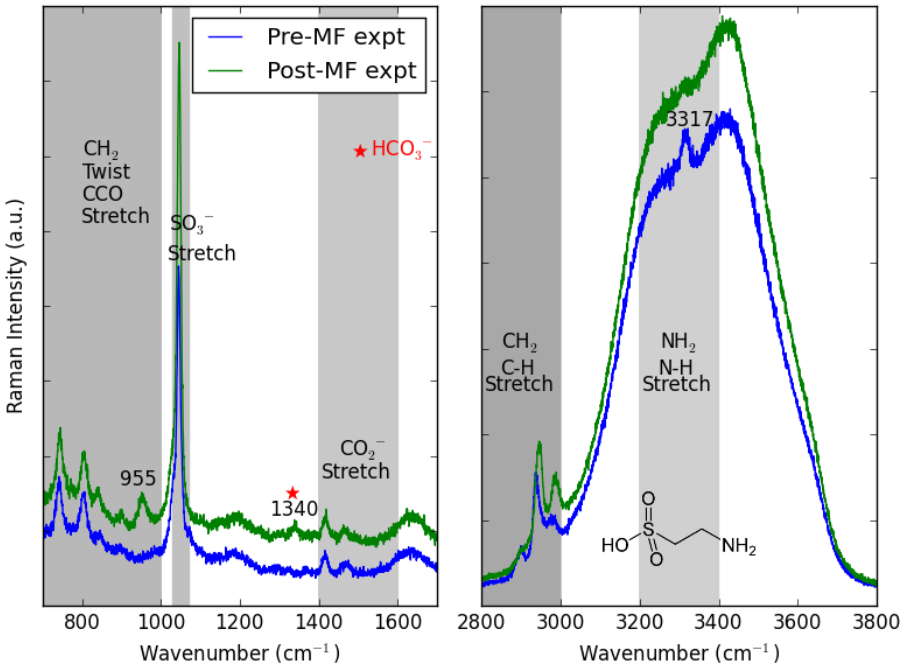

Figure 9: Raman Spectra for TAU.

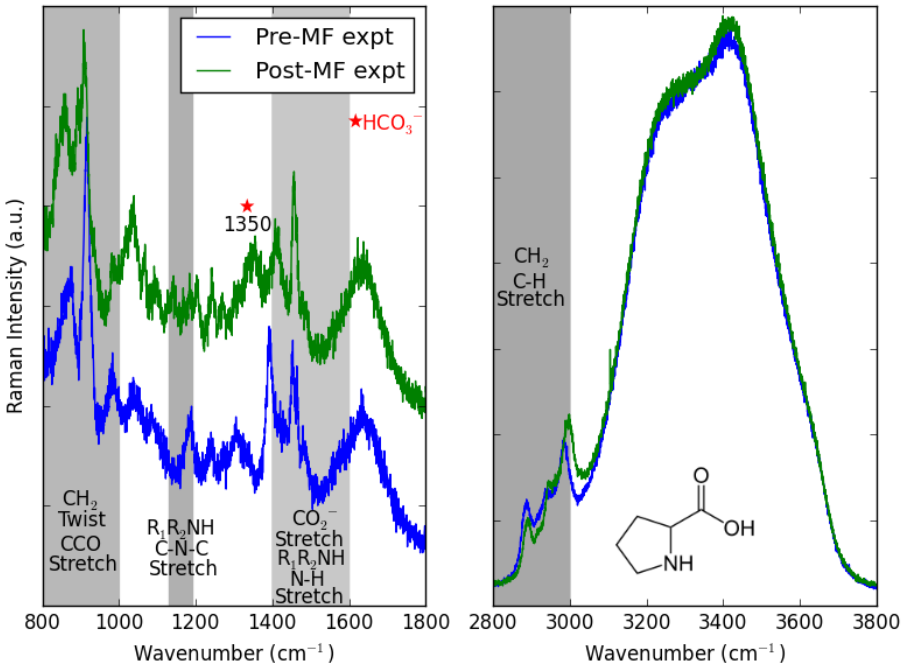

Figure 10: Raman Spectra for PRO.

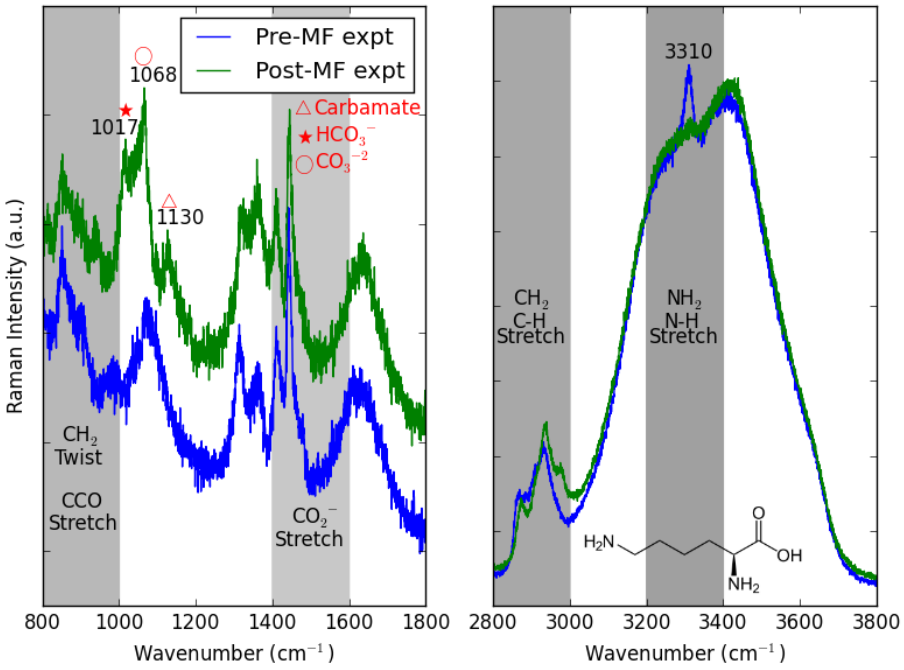

Figure 11: Raman Spectra for LYS.

4. Discussion

Microfluidic absorption experiments provide a rapid, low-volume, and direct quantitative comparison of the CO_2 absorption capacity and absorption rate between several absorbent solutions. The results of this set of experiments shows that the potassium salt of lysine absorbs more CO_2 than the potassium salts of glycine, taurine, or proline as well as more than MEA at the same molar absorbent concentration. This result suggests that the additional primary amine in lysine's side chain contributes additional CO_2 capacity through additional reaction with CO_2 over the solutions containing a solitary amine group per absorbent molecule. However, comparison between

lysine and glycine shows that doubling the number of primary amine groups in the amino acid molecule results in less than a doubling in CO_2 uptake. This is not surprising due to the high pKa (10.53) of the lysine side chain, so as CO_2 is absorbed the decrease in solution pH (initially 11.58) can result in protonation of some of the amine groups and decrease the availability for reaction with CO_2. Never the less the potassium salt of lysine has exhibited a rich CO_2 loading >50% greater than MEA. Consequently we suggest that lysine should receive more attention than the small number of studies [24] it has been included in to date. The potassium salts of glycine and taurine exhibited similar capacity to MEA, while prolinate exhibited the lowest CO_2 capacity. This suggests that the secondary amine group of proline does not lead to an increase in the amount of bicarbonate versus carbamate formed over the cases of the primary amines. Steric hindrance effects may be a contributing factor to the lower rich CO_2 loading of PRO.

While LYS exhibited a slightly longer time to reach its maximum CO_2 loading than the other solutions in this study, the initial absorption rate of LYS was significantly faster than the other amino acid salts and slightly higher than MEA. Which solvent would exhibit the fastest absorption rate in an absorber would vary based on the residence time of CO_2 and the solvent. Certainly at very low residence times, LYS would be an attractive option. The absorption fluxes measured using the microfluidic apparatus are significantly faster than those reported for wetted-wall column experiments (on the order 10^{-5} to 10^{-3} mol/m^{2}s) [8]. However that the flux is significantly greater at the microfluidic length scale is not surprising and consistent with past CO_2 absorption results at similar microfluidic length scales that report

fluxes in the range of 0.98-1.8 mol/m^{2}s depending on the gas space velocity [33]. This highlights the need to limit the comparison of absolute absorption rates to data collected with the same experimental setup.

LYS also exhibited a higher equilibrium CO_2 absorption capacity than MEA in the CSTR experiments. At the same solvent concentrations as in the microfluidic experiments, 1.32 mol CO_2/mol lysine was absorbed compared with only 0.68 mol CO_2/mol MEA. These capacities were measured at a higher (40 vs 23 °C) temperature and lower CO_2 gas pressure than in the microfluidic experiments. The fact that both capacities were found to be significantly higher in the CSTR experiment could be an indication that CO_2 plug volume reduction in the microfluidic reactor is partly controlled by mass-transfer. As is the case with comparing the absorption rates, the absolute values of the CO_2 loadings should only be compared between solutions with the same testing method. However, it is most important that the qualitative trend in the absorption capacity between different solvents (LYS and MEA) that was observed in the microfluidic experiment was also observed in the CSTR experiments. Consequently, the microfluidic experiments described in this work provide a volume and time-efficient means to screen several solvents and identify which one's are the most promising candidate based on absorption capacity prior to more time and volume intensive testing, such as in a CSTR, being done. This advantage is particularly relevant for novel solvents that may be costly to produce in liter-scale quantities prior to their CO_2 capture potential being experimentally investigated.

The results in Table 3 shows that the trends in CO_2 absorption capacity is dependent on whether the solvents are compared on a constant moles of

amine/amino acid basis or constant mass fraction of water basis. Due to the higher molecular weight of lysine vs. MEA, when the molar concentration of lysine and MEA are constant (0.53M) LYS absorbs more CO_2 than MEA, while when the combined lysine/koh mass fraction is kept at 30 wt% to match the MEA benchmark, MEA absorbs more CO_2 than LYS. In order to match the CO_2 absorption capacity of 30 wt% MEA, a higher concentration than 1.48M of potassium lysinate is needed. At higher concentrations, precipitation may introduce additional complexity and to determine the overall effect of replacing MEA with LYS an in-depth analysis would have to be done to take in account the benefits of LYS over MEA(lower volatility, lower corrosivity, lower toxicity, higher CO_2 absorption at same molar concentration of solvent) as well as the drawbacks (higher molecular weight, precipitation of solids). While LYS certainly presents several advantages over MEA, this work also suggests further research into all these competing factors as well as further thermodynamic information regarding regeneration should be done.

Inspection of the Raman spectra of the MEA and amino acid salt solutions before and after CO_2 absorption confirms the occurrence of a reaction and the formation of carbamate, bicarbonate, and carbonate as products. For the primary amines in this study, the occurrence of reaction between CO_2 and the primary amine group is confirmed by the disappearance of the peak at 3310-3320 cm^{-1} which is indicative of N-H stretching in the NH_2 species. In MEA solutions, carbamate, bicarbonate, and carbonate result in peaks at 1162 cm^{-1}, 1017 cm^{-1}, and 1067 cm^{-1} respectively [34]. All three of these peaks are absent in the pre-MF experiment spectrum for MEA and present in the post-MF experiment spectrum. While peaks in the same re-

gion appear in some of the post-MF experiment spectra for the amino acid salts, peaks in other areas appear as well. Post-MF GLY exhibits new peaks at 914 and 1445 cm^{-1} in addition to a broad peak (1045 cm^{-1}) in the region of bicarbonate/carbonate in MEA and a 1175 cm^{-1} peak in the region of carbamate in MEA. Post-MF TAU does not exhibit new peaks in the same region as bicarbonate/carbonate/carbamate in MEA or GLY but exhibits only two new peaks at 955, in the expected range of 930-1100 cm^{-} for NH_3^+ rocking and/or the C-N stretch for NH_3^+ [35], and 1340 cm^{-1}. A peak in the similar range of 1340-1360 cm^{-1} also appears for the case of post-MF PRO and is in a similar region as the CO symmetric stretch of bicarbonate [36, 37]. The spectrum of prolinate undergoes considerable changes in peak positions as a result of CO_2 absorption and is consequently difficult to interpret further. LYS exhibits very similar new Raman peaks in the post-MF experiment spectrum as MEA and GLY with peaks in the 1010-1070 cm^{-1} region indicative of C-OH stretching in bicarbonate and the symmetric stretch of carbonate [37] as well as at 1130 cm^{-1} indicative of carbamate. The shift of the higher peak from 1162 cm^{-1} in MEA and 1175 cm^{-1} in GLY to 1130 cm^{-1} in LYS may indicate a lower bond energy for carbamate in LYS and consequently an equilibrium that favors bicarbonate/carbonate more for the case of LYS than for MEA or GLY.

5. Conclusions

The CO_2 absorption capacity and rate of four amino acid salts was evaluated and compared with MEA through analysis of segmented flow in a microfluidic channel. The CO_2 loading of the absorbent solutions was cal-

culated from the decrease in volume of an entrained CO_2 plug as it traveled through the microfluidic reactor using image analysis. The potassium salt of lysine exhibited the highest rich CO_2 loading, >50% higher than MEA. The potassium salts of glycine and taurine exhibited similar rich loadings to MEA, while the potassium salt of proline exhibited the lowest rich CO_2 loading. The CO_2 absorption capacity of the potassium salt of lysine was then further investigated and compared with MEA in a CSTR.The CSTR results showed that when the molar concentration of MEA and LYS was kept constant at 0.53M, the LYS solution exhibited a >90% higher CO_2 absorption capacity than MEA. However, when the solvents were compared at a constant mass fraction instead of constant molar concentration, MEA absorbed more CO_2 due to its lower molecular weight than LYS. Consequently, the effect of differing molecular weights should always be considered when designing experiments to screen the CO_2 absorption capacity of several absorbents. Raman spectroscopy was used to confirm the occurrence of a reaction and to identify the reaction products. The Raman spectrum of each absorbent solution before the microfluidic experiment was compared with the absorbent solution after exiting the microfluidic reactor. Spectral features consistent with the formation of bicarbonate, carbonate and carbamate were found for all solutions. The results of this work suggest that the potassium salt of lysine should be further investigated as a post-combustion CO_2 capture solvent since it would enable a greater amount of CO_2 to be absorbed for the same moles of absorbent molecule than is the case for MEA, and it has been largely overlooked in previous amino acid salt solution studies. Due to lysine's large molecular weight, the combined mass fraction of lysine/koh would need to be

higher than the 30% that is customary for MEA in order to achieve the same rich CO_2 loading. Determining the optimal capture solution composition for a potassium lysinate process is beyond the scope of the present work. Future investigation of LYS should include regeneration studies, thermal conductivity measurements, and the effect of precipitation in particular. This work also highlights the experimental efficiency and speed of microfluidic reactors as screening tools for evaluating CO_2 absorbents. Trends in CO_2 absorption capacity consistent with those observed in a CSTR can be determined with less than a mL and in substantially shorter time by analyzing images of CO_2 plug dissolution in segmented flow in a microfluidic channel.

6. Acknowledgment

The authors would like to acknowledge Chris Nelson for help in operating the optical hardware and software used in the microfluidic experiments. The authors would like to acknowledge Elliot Roth for conducting the viscosity measurements of the 30 wt% MEA and Potassium Lysinate solutions. The authors would like to acknowledge Nicholas Siefert for insightful discussion and advice in planning the CSTR experiments.

process, or service by trade name, trademark, manufacturer, or otherwise does not necessarily constitute or imply its endorsement, recommendation, or favoring by the United States Government or any agency thereof. The views and opinions of authors expressed herein do not necessarily state or reflect those of the United States Government or any agency thereof."

References

[1] Maria Van der Hoeven. CO_2 emissions from fuel combustion highlights. Technical report, International Energy Agency, 2013.

[2] U.S. EPA. Inventory of u.s. greenhouse gas emissions and sinks: 1990-2012. Technical report, U.S.Environmental Protection Agency, April 2014.

[3] B. Metz. Special report on carbon dioxide capture and storage. Technical report, IPCC, 2005.

[4] Gary T. Rochelle. Amine scrubbing for CO_2 capture. *Science*, 325(5948):1652–1654, 2009.

[5] Alicia J. Reynolds, T. Vincent Verheyen, Samuel B. Adeloju, Erik Meuleman, and Paul Feron. Towards commercial scale postcombustion capture of CO_2 with monoethanolamine solvent: Key considerations for solvent management and environmental impacts. *Environmental Science & Technology*, 46(7):3643–3654, 2012. PMID: 22324566.

[6] Itoro J. Uyanga and Raphael O. Idem. Studies of SO_2- and O_2-induced degradation of aqueous MEA during CO_2 capture from power plant flue

gas streams. *Industrial & Engineering Chemistry Research*, 46(8):2558–2566, 2007.

[7] Alexander K. Voice and Gary T. Rochelle. Oxidation of amines at absorber conditions for CO_2 capture from flue gas. *Energy Procedia*, 4(0):171 – 178, 2011. 10th International Conference on Greenhouse Gas Control Technologies.

[8] Gary Rochelle, Eric Chen, Stephanie Freeman, David Van Wagener, Qing Xu, and Alexander Voice. Aqueous piperazine as the new standard for CO_2 capture technology. *Chemical Engineering Journal*, 171(3):725 – 733, 2011. Special Section: Symposium on Post-Combustion Carbon Dioxide Capture.

[9] J.Tim Cullinane and Gary T. Rochelle. Carbon dioxide absorption with aqueous potassium carbonate promoted by piperazine. *Chemical Engineering Science*, 59(17):3619 – 3630, 2004.

[10] Ujjal K. Ghosh, Sandra E. Kentish, and Geoff W. Stevens. Absorption of carbon dioxide into aqueous potassium carbonate promoted by boric acid. *Energy Procedia*, 1(1):1075 – 1081, 2009. Greenhouse Gas Control Technologies 9 Proceedings of the 9th International Conference on Greenhouse Gas Control Technologies (GHGT-9), 16-20 November 2008, Washington DC, {USA}.

[11] Hanna Knuutila, Hallvard F. Svendsen, and Olav Juliussen. Kinetics of carbonate based CO_2 capture systems. *Energy Procedia*, 1(1):1011 – 1018, 2009. Greenhouse Gas Control Technologies 9 Proceedings of the

9th International Conference on Greenhouse Gas Control Technologies (GHGT-9), 16-20 November 2008, Washington DC, USA.

[12] Tobias Jockenhoevel, Ruediger Schneider, and Helmut Rode. Development of an economic post-combustion carbon capture process. *Energy Procedia*, 1(1):1043 – 1050, 2009. Greenhouse Gas Control Technologies 9 Proceedings of the 9th International Conference on Greenhouse Gas Control Technologies (GHGT-9), 16-20 November 2008, Washington DC, {USA}.

[13] J. van Holst, G.F. Versteeg, D.W.F. Brilman, and J.A. Hogendoorn. Kinetic study of with various amino acid salts in aqueous solution. *Chemical Engineering Science*, 64(1):59 – 68, 2009.

[14] Subham Paul and Kaj Thomsen. Kinetics of absorption of carbon dioxide into aqueous potassium salt of proline. *International Journal of Greenhouse Gas Control*, 8(nil):169–179, 2012.

[15] Eva Sanchez Fernandez, Katarzyna Heffernan, Leen V. van der Ham, Marco J. G. Linders, Emma Eggink, Frank N. H. Schrama, D. W. F. Brilman, Earl L. V. Goetheer, and Thijs J. H. Vlugt. Conceptual design of a novel CO_2 capture process based on precipitating amino acid solvents. *Industrial & Engineering Chemistry Research*, 52(34):12223–12235, 2013.

[16] Yamini Sudha Sistla and Ashok Khanna. Carbon dioxide absorption studies using amine-functionalized ionic liquids. *Journal of Industrial and Engineering Chemistry*, 20(4):2497 – 2509, 2014.

[17] Jin-ah Lim, Dong Hyun Kim, Yeoil Yoon, Soon Kwan Jeong, Ki Tae Park, and Sung Chan Nam. Absorption of CO_2 into aqueous potassium salt solutions of l-alanine and l-proline. *Energy & Fuels*, 26(6):3910–3918, 2012.

[18] Robert J. Hook. An investigation of some sterically hindered amines as potential carbon dioxide scrubbing compounds. *Industrial and Engineering Chemistry Research*, 36(5):1779–1790, 1997.

[19] A.F. Portugal, P.W.J. Derks, G.F. Versteeg, F.D. Magalhães, and A. Mendes. Characterization of potassium glycinate for carbon dioxide absorption purposes. *Chemical Engineering Science*, 62(23):6534 – 6547, 2007.

[20] Quanzhen Huang, Saloni Bhatnagar, Joseph E. Remias, John P. Selegue, and Kunlei Liu. Thermal degradation of amino acid salts in CO_2 capture. *International Journal of Greenhouse Gas Control*, 19:243 – 250, 2013.

[21] P. S. Kumar, J. A. Hogendoorn, G. F. Versteeg, and P. H. M. Feron. Kinetics of the reaction of CO_2 with aqueous potassium salt of taurine and glycine. *AIChE Journal*, 49(1):203–213, 2003.

[22] Hanna Knuutila, Ugochukwu E. Aronu, Hanne M. Kvamsdal, and Actor Chikukwa. Post combustion CO_2 capture with an amino acid salt. *Energy Procedia*, 4(0):1550 – 1557, 2011. 10th International Conference on Greenhouse Gas Control Technologies.

[23] Ho-Jun Song, Sangwon Park, Hyuntae Kim, Ankur Gaur, Jin-Won Park, and Seung-Jong Lee. Carbon dioxide absorption characteristics of aque-

ous amino acid salt solutions. *International Journal of Greenhouse Gas Control*, 11(0):64 – 72, 2012.

[24] Benedict Mai Lerche. *CO_2 Capture from Flue gas using Amino acid salt solutions*. PhD thesis, Technical University of Denmark, August 2012.

[25] Milad Abolhasani, Mayank Singh, Eugenia Kumacheva, and Axel Gunther. Automated microfluidic platform for studies of carbon dioxide dissolution and solubility in physical solvents. *Lab Chip*, 12:1611–1618, 2012.

[26] Ruopeng Sun and Thomas Cubaud. Dissolution of carbon dioxide bubbles and microfluidic multiphase flows. *Lab Chip*, 11:2924–2928, 2011.

[27] A. Gunther M. Abolhasani, E. Kumacheva. Model-predictive strategy for exploration of carbon dioxide dissolution and mass transfer.

[28] Stephanie G. R. Lefortier, Peter J. Hamersma, Andre Bardow, and Michiel T. Kreutzer. Rapid microfluidic screening of CO_2 solubility and diffusion in pure and mixed solvents. *Lab Chip*, 12:3387–3391, 2012.

[29] Wei Li, Kun Liu, Ryan Simms, Jesse Greener, Dinesh Jagadeesan, Sascha Pinto, Axel Gunther, and Eugenia Kumacheva. Microfluidic study of fast gas-liquid reactions. *Journal of the American Chemical Society*, 134(6):3127–3132, 2012. PMID: 22176612.

[30] Chunying Zhu, Chunfang Li, Xiqun Gao, Youguang Ma, and Dongzhi Liu. Taylor flow and mass transfer of CO_2 chemical absorption into MEA aqueous solutions in a t-junction microchannel. *International Journal of Heat and Mass Transfer*, 73(0):492 – 499, 2014.

[31] Lu Yang, Jing Tan, Kai Wang, and Guangsheng Luo. Mass transfer characteristics of bubbly flow in microchannels. *Chemical Engineering Science*, 109(0):306 – 314, 2014.

[32] Dan Voicu, Milad Abolhasani, Rachelle Choueiri, Gabriella Lestari, Caroline Seiler, Gabriel Menard, Jesse Greener, Axel Guenther, Douglas W. Stephan, and Eugenia Kumacheva. Microfluidic studies of CO_2 sequestration by frustrated Lewis pairs. *Journal of the American Chemical Society*, 136(10):3875–3880, 2014. PMID: 24555752.

[33] Chunbo Ye, Guangwen Chen, and Quan Yuan. Process characteristics of CO_2 absorption by aqueous monoethanolamine in a microchannel reactor. *Chinese Journal of Chemical Engineering*, 20(1):111 – 119, 2012.

[34] P.A. Gamunu L. Samarakoon, Niels H. Andersen, Cristina Perinu, and Klaus-J. Jens. Equilibria of MEA, DEA and AMP with bicarbonate and carbamate: A Raman study. *Energy Procedia*, 37(0):2002 – 2010, 2013. GHGT-11.

[35] *Infrared and Raman Characteristic Group Frequencies: Tables and Charts*. John Wiley & Sons Ltd., 2001.

[36] Nanping Wen and Murray H. Brooker. Ammonium carbonate, ammonium bicarbonate, and ammonium carbamate equilibria: A Raman study. *The Journal of Physical Chemistry*, 99(1):359–368, 1995.

[37] John D. Frantz. Raman spectra of potassium carbonate and bicarbonate

aqueous fluids at elevated temperatures and pressures: Comparison with theoretical simulations. *Chemical Geology*, 152(3-4):211 – 225, 1998.